Appl. Phys. B (2013) 112:133–142
DOI 10.1007/s00340-013-5409-2

Applied Physics B
Lasers and Optics

Stabilization of center frequency nanowell metamaterials for SERS applications

Zachary A. Sechrist · Ronald J. Tonucci · Lee R. Cambrea

Received: 7 September 2012 / Accepted: 8 March 2013 / Published online: 12 April 2013

Abstract A finite element solver is used to design a metamaterial structure with large and stable Raman scattering enhancement. The metamaterial consists of an array of tapered nanowells etched into a metal/dielectric multilayer stack. The plasmonic activity as a function of the number of layers and sidewall angle of the nanowell is investigated. As the nanowell side wall angle is increased, the tops of the nanowells are drawn closer together, greatly increasing the local electric field intensity. The taper is designed such that the patterned layers at the bottom of the nanowell would have a negative refractive index if isolated from the stack, and patterned layers at the top of the stack would have a positive refractive index if isolated from the stack. Simulations predict that coupled layers at the bottom of the tapered nanowell, exhibiting a negative refractive index, experience a blue shift in local resonant frequency as the well diameter is increased or the period is decreased. The upper layers, with positive refractive index, exhibit a red shift as the well diameter is increased or the period is decreased. These opposing responses stabilize the resonant frequency with respect to variations in diameter and periodicity commonly encountered with nanofabrication techniques.

Z. A. Sechrist (✉) · L. R. Cambrea
NAWCWD, 1900 Knox St., Stop 6303, China Lake, CA 93555, USA
e-mail: zachary.sechrist@navy.mil

R. J. Tonucci
NRL, 4555 Overlook Ave SW, Washington, DC 20375, USA

1 Introduction

Surface enhanced Raman scattering (SERS) has become one of the most studied plasmonic applications to date because of the unparalleled sensitivity and selectivity of the technique. Inelastic Raman scattering, an inherently insensitive process, can be enhanced by as much as 14 orders of magnitude through electromagnetic coupling between the molecule of interest and a plasmonic surface [1]. The majority of scientific research in the field has been focused on increasing the performance of the plasmonic surface. Two major thrusts for SERS surface research have been the increase in the localized electric field strength, and the reproducibility/uniformity of the field enhancement across the surface. These two thrusts appear to compete against one another in experimental demonstrations, leading to the relationship known as the "SERS uncertainty principle" [2]:

$$\text{substrate uniformity} \times \text{enhancement factor} \approx \text{constant} \quad (1)$$

The first observations of large Raman scattering enhancements were on substrates with roughened metal surfaces. The enhancements, at least partially, were attributed to an electromagnetic mechanism. Under this mechanism, the amount of energy coupled into and out of surface bound analytes was magnified by the local electric field. The electric field intensity at the tip of a rough spot would be considerably higher due to the "lightening rod" effect [3]. These localized points of huge field strength, known as hot spots, gave rise to large Raman scattering enhancement. In accordance with the SERS uncertainty principle, these sharp points created from surface roughening suffered from problems with uniformity. Surface roughening would randomly produce sharp points that delivered high enhancement factors (EF). These random

high EF points were surrounded by a low EF area, such that surface averaged enhancement was only a fraction of the sharpest point EF. In addition, surface stability posed a significant challenge. The EF from an SERS surface is highly dependent on nanoscale feature geometry [4], but fine features tend to be sensitive towards various chemical, high field, and temperature environments [5].

A more recent approach for Raman enhancement has been demonstrated by dispersion engineering through surface modification. By systematically adding or subtracting surface features, it is possible to tune the plasmonic response of the surface. Common types of modified surfaces are photonic crystals and metamaterials. By modifying the dispersion of the surface, it is possible to maximize the plasmonic activity at a select wavelength, and thus maximize the EF of the surface for a particular molecule. These surfaces are generally periodic structures, so the enhancement is uniformly distributed at the scale of the period. However, these engineered lattices can have strong nearest neighbor interactions that make the average EF susceptible to disorder, greatly reducing Raman performance [6, 7]. Although the resolution of nanofabrication techniques is constantly improving, disorder in the fabrication of nanoscale structures suitable for SERS is still highly probable. Therefore, an error-tolerant design is highly desirable.

Multilayer resonators have previously been studied for dispersion engineering in the field of metamaterials [8, 9], and show promise in the field of SERS [10, 11]. This study focuses on a multilayer resonator design because of the excellent dispersion tunability of the system. The modeled material in this paper is similar to the 3D fishnet metamaterial structure proposed by Valentine [12]; however, the rectangular holes of the previous work are replaced with tapered circular holes that extend through the metal/dielectric layers. The unit cell can be seen in Fig. 1. The repeating unit cell design distributes the electric field across the *x*,*y*-plane, effectively spreading the enhancement across the substrate to improve the signal uniformity. These circular holes were modeled with varying degrees of side wall angle and will be referred to as tapered nanowells for the remainder of the article.

Increased nanowell taper not only generates a stack of graded resonator geometries, the structure also has potential to produce significant localized electric field enhancements. By increasing the side wall angle to the extent that the adjacent nanowells in an array are almost touching, it is possible to explore the compliment of nearly touching plasmonic spheres. The investigation into the electric field enhancement between two closely spaced spheres has been explored previously [13, 14]. These previous works demonstrated that the electric field was greatest when the gap between adjacent spheres was very small. According to the Babinet principle, complimentary systems produce resonances at close to the same frequency and of similar strength [15]. Therefore, because the closely spaced spheres produced a significant EF, one would also expect a high EF from a complimentary void structure. In addition, Raman scattering enhancement from concave versus convex structures has been studied theoretically, in which the concave voids were shown to have superior performance [16].

If the tapered nanowells are allowed to overlap, the top metal ring becomes discontinuous. In this case, lower layers still closely resemble the high electric field enhancement from the closely spaced voids, while the top layer now mimics the shape and function of a bowtie nanoantenna. Bowtie structures have also been reported in recent publications to produce significant local field enhancements [17, 18]. Again this structure was predicted to produce an SERS hot spot.

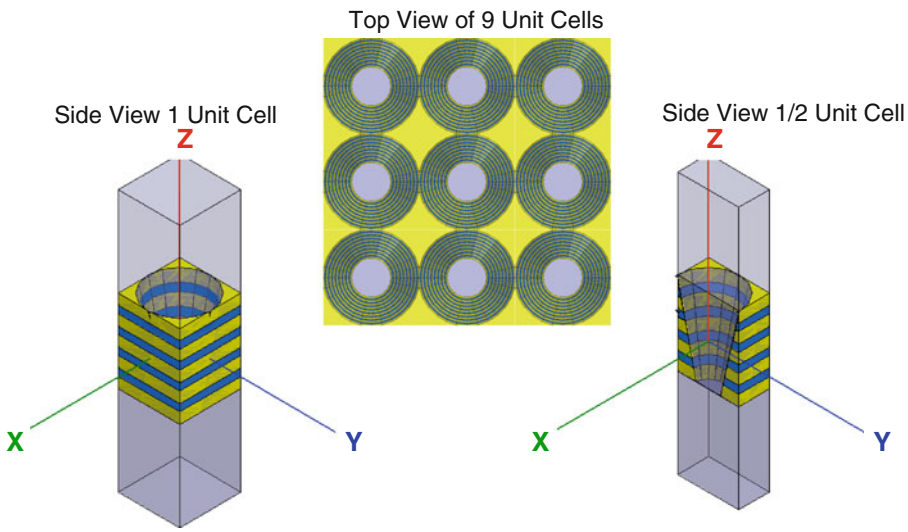

Fig. 1 Images of the nanowell surface etched into a metal/dielectric multilayer stack. The *yellow* layers represent gold, the bright *blue* layer is aluminum oxide, and the nanowell structure sits atop a *grey* glass substrate

In the case of both nearly touching nanowells and the slightly overlapped nanowells, the electric field intensity was highest when their respective gaps were very small. This represents a big problem as very small gaps are difficult to fabricate reproducibly, and small variance can lead to a significant resonance frequency shift. The gap sensitivity is a perfect example of the SERS uncertainty principle, as the higher performance structure is more likely to have poor uniformity. The multilayer tapered nanowell array is uniquely well adapted to overcome this problem. The multilayered nanowell with large side wall angle exhibits very large enhancements and is stable with respect to potential fabrication errors due to coupling between progressively lower effective refractive index resonators stacked atop one another.

2 Model description

A commercial finite element solver, High Frequency Structural Simulator (HFSS) from Ansys corp., was used to solve Maxwell's equations. The 3D full-wave electromagnetic solver was tested with literature examples to validate the accuracy of the approach. Absorptance was calculated from the simulation scattering parameters, and related to the Raman intensity [19]:

$$I_{\mathrm{SERS}} \propto A(f_{\mathrm{L}}) \times A(f_{\mathrm{S}}) \tag{2}$$

$A(f_{\mathrm{L}})$ = Absorptance at the excitation frequency, $A(f_{\mathrm{S}})$ = Absorptance at the Raman shifted frequency.

Only one plasmonic resonance was used to interact with both frequencies, so the plasmon resonant frequency was tuned to occur between the excitation and Raman shifted absorption frequencies. The excitation and Raman shifted wavelengths were close, so the SERS intensity was roughly proportional to the square of the plasmon absorptance. This simplified approach ignored the change in dielectric constant of the metal between the two frequencies and did not account for the coupling efficiency between the plasmon wave and the molecular dipole. However, this approach has been used in the literature to predict plasmonic activity in nanovoids previously [20]. In the case of benzenethiol, a common SERS analyte, the laser excitation was $\lambda =$ 785 nm, the Raman shift was 1073 cm^{-1} ($\lambda =$ 857 nm), thus the target plasmon resonance was $\lambda =$ 821 nm or $f_{\mathrm{P}} =$ 365 THz. The first-order resonant peak position was optimized to occur at $\lambda =$ 821 nm by adjusting the periodicity and layer thicknesses. The first-order peak was more stable with respect to changes in the period and nanowell radius. Using the first-order resonance also forced the array period to be smaller, allowing a higher nanowell hot spot packing density.

A schematic of the modeled surface is shown in Fig. 1. The substrate was glass with the real part of the dielectric constant $\mathrm{Re}(\varepsilon_{\mathrm{glass}}) = 2.35$. The surrounding environment was assumed to be air $\mathrm{Re}(\varepsilon_{\mathrm{air}}) = 1$. The blue layers represented aluminum oxide, $\mathrm{Re}(\varepsilon_{\mathrm{Al_2O_3}}) = 2.72$. The imaginary component of all three dielectric materials was assumed to be zero. The yellow layers were gold, and were described by a complex dispersion relationship [21]:

$$\varepsilon_{\mathrm{Au}} = 1 - \frac{f_{\mathrm{p}}^2}{f(f + i\Gamma)} \tag{3}$$

$\varepsilon_{\mathrm{Au}}$ = complex dielectric constant for gold, f_{p} = plasma frequency = 2.1×10^{15} Hz, Γ = scattering frequency = 1.9×10^{13} Hz.

The nanowells were arranged in a square lattice with a period of 345 nm. Incident radiation was polarized, with the electric field vector pointing in the *y*-direction, and the wave vector aligned parallel with the surface normal (negative *z*-direction). The alumina layers were 41 nm thick, and the gold layers were 60 nm thick. Optimization of the structure was performed using a quarter of the nanowell unit cell to expedite the process. Tapered nanowells all had the radii at the bottom of the well set at 70 nm, while the radii at the top of the wells were varied. The nanowell design assumes the well extends through all of the gold and alumina layers. Over etching into the substrate was examined. Over etching the well into the substrate shifted the resonance, but did not have deleterious effects on the strength or bandwidth of the plasmonic activity.

3 Results and discussion

One of the most striking aspects of the nanowell design is the use of multiple metal and dielectric layers. It was previously shown that layering a metal nanodisk led to a two times increase in scattering intensity [11]. In this paper, we first compare solid and layered void arrays. The simulated absorptance spectra for identical nanowell geometries, one array etched into a solid gold substrate and the other array etched into a multilayered substrate containing nine gold layers, are compared in Fig. 2. Indeed, identical nanowell structures etched into a solid gold substrate versus a multilayer gold and alumina substrate exhibit very different plasmonic responses. The multilayered sample has nearly three times the peak absorptance, making the predicted SERS intensity almost nine times stronger. This increased absorption is generated by the increased density of plasmonic surfaces in the multilayered system. In addition, the absorption peak is much broader. The additional bandwidth in the multilayered system can be partially attributed to the

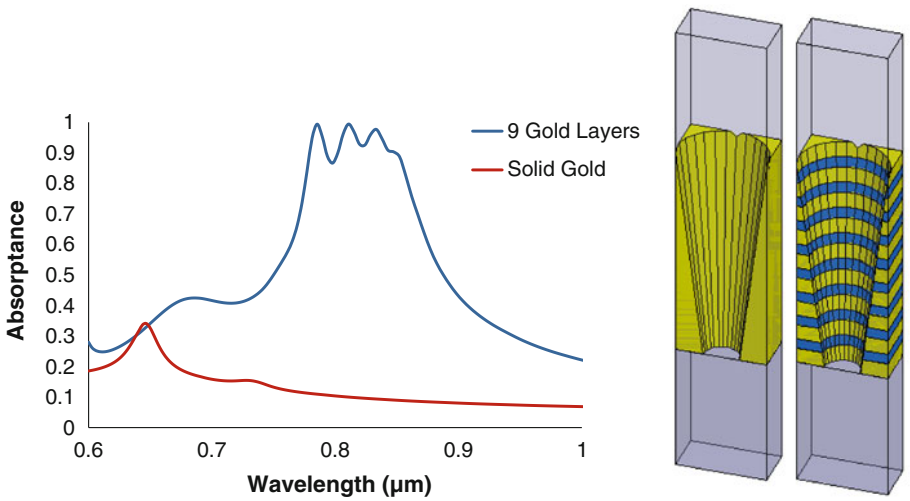

Fig. 2 A comparison of absorptance spectra from identical well geometries etched into solid gold (*red*), and a gold/aluminum oxide multilayer (*blue*). In both tapered nanowell structures the bottom radius is 70 nm, the top radius is 175 nm, the array period is 345 nm, and the total well depth is 868 nm

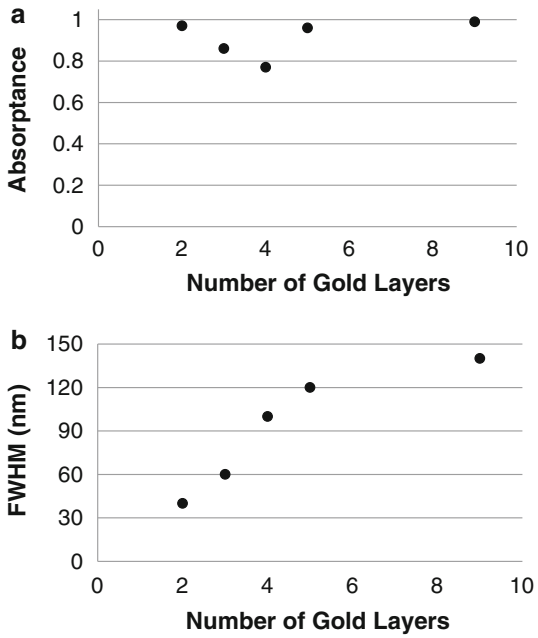

Fig. 3 A comparison of the **a** absorptance intensity, and **b** bandwidth, as a function of the number of multilayers in the gold/aluminum oxide stack. The thickness of the individual layers was held constant: gold = 60 nm, and aluminum oxide = 41 nm. The top radius of the nanowell was held constant at 175 nm, and the bottom radius was held constant at 70 nm, while the depth of the well was allowed to vary with the number of layers

individual layers within the system inductively coupling to one another, but we will also show later in this paper that the dissimilarity between layers vertically stacked atop one another adds to the absorption breadth observed. The wavelength position of the layered structure absorption peak is red shifted compared with the solid well. A red shift in the resonant peak as a function of the number of multilayers has been reported previously [11]. The shift is attributed to plasmon coupling between the gold layers.

Although the difference between the spectra of periodic arrays of layered metal and solid metal nanowells is quite dramatic (Fig. 2), the difference in peak absorptance intensity as a function of the number of layers is relatively low. Absorptance as a function of the number of layers is shown in Fig. 3a. In these simulations, the nanowell array period was 345 nm, and each layer thickness was constant with Au = 60 nm and Al_2O_3 = 41 nm. Each of the gold layers was separated by an alumina spacer layer. By adding gold layers, the total height of the nanowell stack was increased. The top and bottom radii of the tapered nanowell were held constant at 175 and 70 nm, respectively. Decreasing the nanowell top radius drastically reduced the absorptance of the multilayers structures (not shown). The peak absorptance intensity initially decreased as the structure was tuned from 2 gold layers to 3 layers, and again decreased to 4 layers. When the fifth gold layer was added, the structure absorbed almost all of the light at the resonant frequency. As more layers were added, the peak absorptance remained very strong (abs $\sim$ 1). The fluctuations in the absorptance strength arose from conflicting influences found in the multilayered structure. Adding layers would effectively increase the density of absorbers. Increasing the density of absorbers would clearly raise absorptance. On the other hand, increasing the number of closely spaced gold layers can decrease total stack absorptance due to destructive interference between the symmetric and anti-symmetric resonant modes [22]. Increasing the number of layers led first to a decrease in absorptance, then to an increase, as these two conflicting influences exchange dominance in this unique system.

The breadth of the absorption peak is shown in Fig. 3b as the full-wave half max (FWHM) of the absorption peak. Although the sample absorptance spectra were not described as a Gaussian, or any other simple curve shape, comparing the FWHM did represent the general peak broadening well. The absorption peak FWHM increased with the number of gold layers. The broader absorption peak extends the wavelength range which could excite, or

be enhanced by, the surface plasmon. This extended range allows a single nanowell surface to enhance scattering from analytes with a Raman absorption anywhere in the plasmonic range, and increases fabrication error tolerance against a shift in the peak's spectral location. Since the sample with nine gold layers (and eight alumina layers) displayed excellent behavior that sample was chosen as the target structure that would be optimized in simulations.

The location and magnitude of the electric field within the nanowell structure as a function of nanowell side wall angle is displayed in Fig. 4. These cross section views of the periodic array unit cell show the electric field at 363 THz ($\lambda = 825$ nm). The incident wave electric field was polarized out of the page. When the walls were nearly vertical, such as the top $r = 90$ nm image, the electric field was evenly distributed in the z-direction. As the angle of the tapered nanowell was increased, the topmost region between the nanowells was narrowed and the electric field intensity in that region increased. The electric field enhancement is similar to that of the nearly touching spheres, in that the most narrow cavity separation produces the largest field strength; hence, the largest SERS enhancement.

Spectra simulated for a metal/dielectric multilayer nanowell array with increasing side wall angle are shown in Fig. 5. The black vertical line represents the target absorption wavelength for benzenethiol, a well characterized material typical in SERS experiments. The bottom radius of the tapered nanowells was held constant at 70 nm. As the side wall angle was increased, the radius of the nanowell top increases from 70 to 180 nm, and the peak absorptance grew from 0.12 to 0.96. The absorptance, and therefore the predicted SERS EF, increased with increasing sidewall angle.

The simulation data in Fig. 5 show that all of the structures were predicted to give some enhancement. The absorption bandwidth of the array of tapered nanowells increased with sidewall angle. Because the nanowell array period was 345 nm, the nanowell array with a top radius = 170 nm was almost overlapped with its nearest neighbor nanowells and the nanowell array with a top radius = 180 nm was overlapped with its nearest nanowell neighbors. It can be seen that the simulation with the slight nanowell overlap yielded the largest absorptance over the widest spectral range with the most improved surface performance.

The increased absorption bandwidth displayed by the multilayered nanowell structure is attributed to both resonator coupling, and dissimilar resonator geometries constructively added to one another. Each gold-alumina-gold sandwich can be modeled as an individual optical LC (inductor-capacitor) circuit resonator [23]. The coupled resonator stack array modeled for Fig. 5 had eight closely spaced gold-alumina-gold resonators. The individual layers were coupled to each other through mutual inductance, and this coupling increased the resonator bandwidth [24]. In addition, the array of closely spaced nanowells found increased plasmonic bandwidth due to nearest neighbor coupling effects in the x,y-plane [25].

As the sidewall angle increased in the nanowell array, there was an increase in absorption bandwidth and the

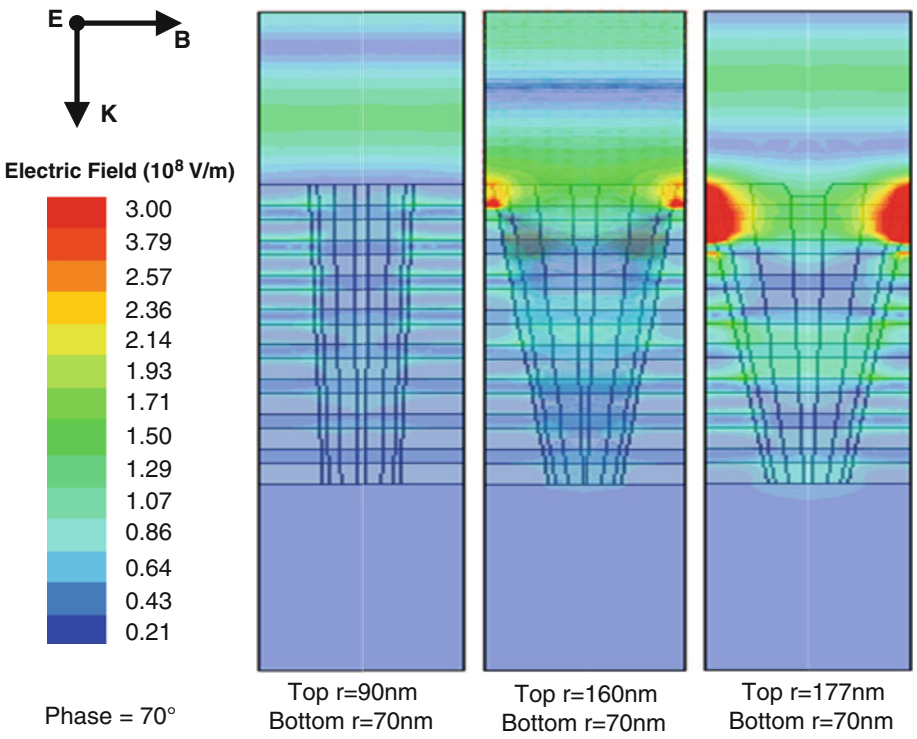

Fig. 4 Electric field strength overlaid on the nanowell structure cross section

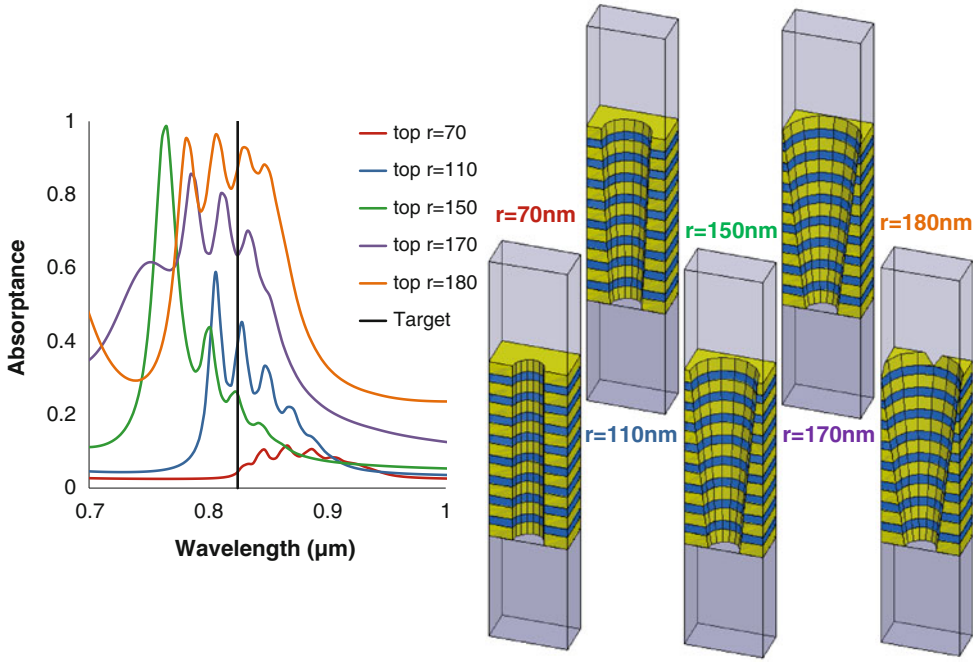

Fig. 5 Absorptance spectra of a nanowell etched into a multilayer nanowell with eight coupled resonators and a well depth of 868 nm. The side wall was varied by holding the radius of the *bottom* of the nanowell constant ($r = 70$ nm), and varying the radius of the *top* of the nanowell. The array period was held constant for all cases at 345 nm. Images of the resulting structures are shown in cross section

electric field strength in each nanowell. In addition, Fig. 5 shows a fascinating shift in the absorption peak wavelength position. There was a decrease (blue shift) in absorption peak wavelength position as the nanowell top radius was increased from 70 nm to 110 nm to 150 nm. Then, the absorption peak position moved towards longer wavelength (red shift) as the radius of the top of the nanowell was further increased from 150 nm to 170 nm to 180 nm. These opposing responses towards an increasing top radius of a nanowell is attributed to the change in the refractive index of the individual resonators inside the stack whose radii, and therefore effective refractive index, changed with each increasing step of the nanowell's top radius.

To elucidate the contributions from the individual resonators on both the spectral position and the spectral bandwidth of the nanowell absorption peak, individual resonators whose geometry matches some section of the tapered nanowell were examined independently. The absorptance spectra from arrays of individual resonators (Au–Al_2O_3–Au layers), and an array eight vertically coupled resonators in a nanowell stack (9 Au layers and 8 Al_2O_3 layers), are shown in Fig. 6. In this figure, the black curve represents a vertically coupled resonator stack array with tapered circular holes etched out of the multilayer. The tapered nanowell radius ranged from 70 nm at the bottom to 180 nm at the top. On the other hand, the individual resonators did not have any taper. The individual resonators consisted of an array of wells etched into metal-dielectric-metal layers. They had the same hole radius through all three layers, and were investigated without any interactions with other resonators in the vertical direction. Adding the individual resonators together does not sum to the eight coupled resonator tapered nanowell spectra, but a comparison of the coupled stack nanowell spectra and the individual resonators does lend insight into the additive role of the vertically stacked individual resonators towards the whole. The coupled stack spectra shows four peaks with shapes similar to the individual resonators, and the breadth of the coupled stack absorption peak is comparable to the total bandwidth spanned by the series of resonators.

Upon closer inspection of the individual resonator spectra, it is observed that the peak absorptance for individual resonators with smaller radii blue shifted with increasing hole radius (resonator with hole radius 70, 110, 150 nm). This effect is in direct contradiction to previous observations of isolated nanoholes with increasing radius [26]. This contrary blue shift was attributed to the periodic composite of tapered nanowells acting as a plasmonic crystal. The plasmonic crystal behavior is determined by not only individual nanowell geometry, but also by the effective refractive index of the entire array. The increased well diameter can red shift the resonant wavelength due to increased cavity size, and nearest neighbor coupling effects. Counteracting the red shift is a dramatic change in the effective refractive index as the nanowell diameter increased.

The individual two gold layer resonators created an artificial magnetism [27], which resulted in a negative permeability. The composite fishnet also had considerable metal fill fraction, leading to a negative permittivity. This type of material has been labeled a double negative material because of these traits, and is characterized as a negative index metamaterial (NIM). The magnitude of the effective refractive index in the NIM is strongly tied to the resonator

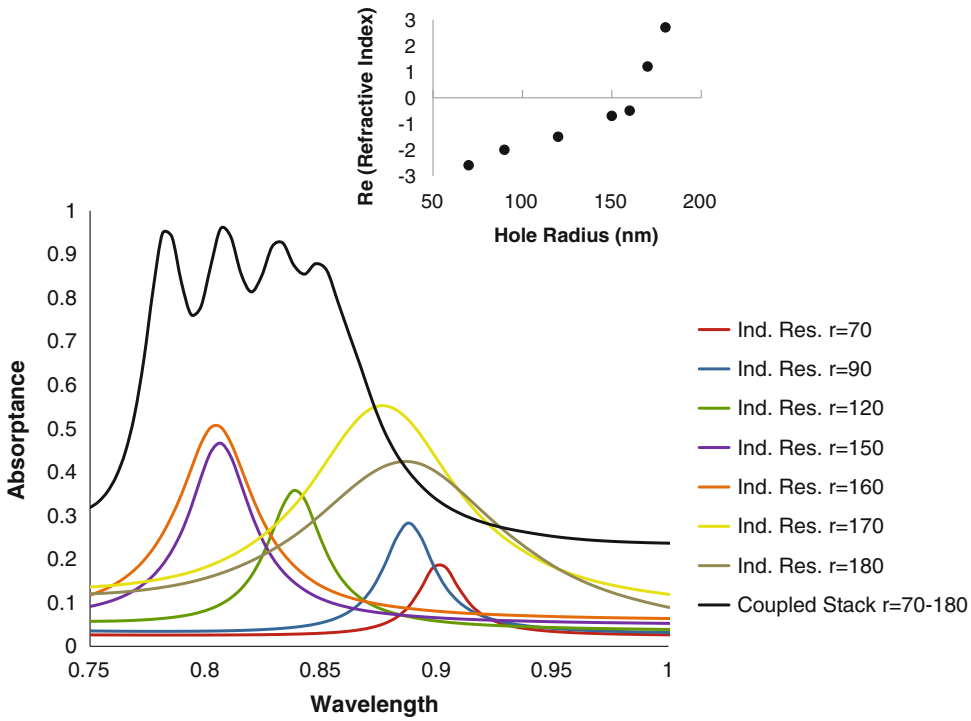

Fig. 6 Absorptance spectra for arrays of various individual gold-alumina-gold resonators with different radii, and the spectra for a multilayered nanowell which had radii that spanned all of the individual resonator radii are displayed. The inset figure shows the effective refractive index value at peak absorptance for the individual resonators

design, thus small changes to the resonator geometry can lead to significant changes in the effective refractive index. The refractive index was de-embedded from HFSS scattering parameters in accordance with literature procedures [28]. The inset in Fig. 6 shows the effective refractive index at resonance. The real part of the refractive index transitioned from $n = -2.6$ in a resonator with radius $= 70$ nm to $n = +2.7$ in a resonator with a radius of 180 nm. The effective refractive index of the entire stack was a low value of only $+0.4$. As the refractive index goes from negative through zero to positive, the absolute value of the real part of the refractive index gets smaller, and then larger. Assuming the resonance position is proportional to the absolute value of the refractive index [29], the peak position of an individual resonator would blue shift and then red shift with increasing well diameter. Affirmation of this behavior in the individual resonator simulations (Fig. 6) suggests that this plasmonic crystal effect is playing a major role in the position of the plasmonic resonance.

The summation of these coupled resonators not only leads to a broad absorption peak, but also the peculiar wavelength position shifting of the nanowell absorption peaks seen in Fig. 5. As the coupled resonator nanowell structure in Fig. 5 has the top radius of the well expanded, the cumulative behavior of the structure adds a larger positive component to an initially negative effective refractive index structure. As the absolute value of the refractive index decreased, the absorption peak blue shifted. After sufficient nanowell radius expansion has pushed the effective refractive index of the multilayer system to zero, adding additional positive index character will increase the absolute value of the refractive index, leading to a red shift. The authors do not claim that the index is the only determining factor in the absorption peak location, but that the increase/decrease in the absolute value of the real part of the refractive index change does play a major role in red/blue shifting the peak location.

The particular choice of nanowell taper parameters in this example generated individual resonator geometries with effective refractive indices spanning both positive and negative values. These positive and negative index resonators display opposing responses to common types of nanofabrication error. The positive resonators that would be located near the top of the nanowell experience a red shift in resonant frequency when the radii of those resonators are increased. The negative resonators that would be located near the bottom of the nanowell experience a blue shift in resonant frequency when the radii of those resonators are increased. The opposing contributions to the resonant frequency of the coupled metamaterial structure combine to result in a very stable frequency response as a function of varying hole radius during fabrication and processing.

Stability, with respect to periodicity disorder, stems from the same oppositional responses from the negative and positive index resonators. As the period increased, the positive index resonators near the top of the nanowell experienced a decrease in positive refractive index value. Therefore, the positive refractive index resonator with increased well to well spacing had a decrease in the absolute value of the effective refractive index and a blue shift in the resonant frequency. The resonators at the

bottom of the nanowell experienced a decrease in the already negative effective refractive index, and therefore an increase in the absolute value of the effective refractive index. The resonators at the bottom of the nanowell will have a red shift in resonant frequency counteracting the positive index resonators at the top of the nanowell to sum a resonant frequency stable graded index resonator stack with respect to periodicity.

Figure 7a–d shows the spectral response of multilayer nanowell arrays towards variation in both the well radius etched into the multilayer, and well to well spacing. To demonstrate the stability created by the gradient of individual resonators found in the tapered nanowell, the tapered nanowell system was compared with a straight walled nanowell in an identical metal/dielectric stack. To maximize the absorptance strength of the straight walled nanowell, the diameter of the well void was 175 nm, and the array period was 345 nm. It can be seen in Fig. 7 that the high absorptance bandwidth is broader in the tapered system because of the response of the coupled dissimilar resonators. In the case of both void radius and array periodicity, the plasmonic response of the tapered system remained very stable. The location of the first order absorption peak of the straight walled nanowell, on the other hand, changed wavelength position rather dramatically for changes in array period and well radius. In a large array that is subject to nanofabrication error, it is assumed that the averaged plasmonic response will be the additive response from many nanowells that would have variation in the radius and period comparable to the variation explored in Fig. 7. The tapered nanowell system displays a clear advantage under these circumstances, as all of the nanowells within the values explored would constructively add the same high intensity response through the desired plasmonic range. The straight walled nanowell, on the other hand, would wash out the plasmonic response due to the summation of dissimilar spectra from the slightly modified geometries.

The coupling of individual negative and positive effective refractive index resonators in a tapered nanowell array created spectral stability with respect to fabrication errors. To quantify and compare the stability, the shift of the first order peak of four nanowell designs were collected: both with and without sidewall angle, and solid metal vs. metal/dielectric stacks. The radii of the angled nanowell varied from 70 nm at the bottom, to 175 nm at the top. Since the nearly touching voids produced the largest electric field intensity, the radii of all of the holes were held constant at 175 nm in the straight walled nanowells. Error in the nanowell radius and array period were investigated, and shown in Table 1. Tolerance was measured as the wavelength shift of the resonant absorption peak given a small change in the designated variable. On inspection of Table 1, it becomes apparent that the side wall angled multilayer structure is more stable relative to disorder compared with all other test cases. The wavelength shift stability is attributed to counter balancing red and blue spectral shifts of the tapered nanowell. The tapered nanowell creates a hot spot that reaches peak intensity when the nanowells were just barely overlapped, but remains present within the 2.9 % disorder for the period and radius. All of the investigated structures became more stable to

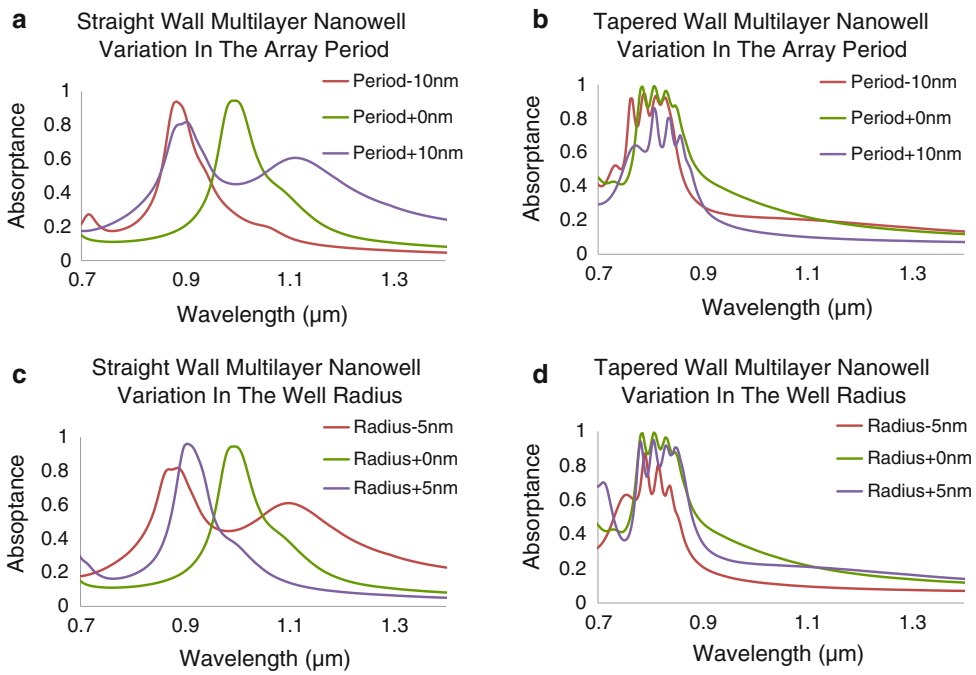

Fig. 7 Comparison of spectra simulated for a coupled resonator stack with straight and angled walls with variation in the array period and nanowell void radius. Both systems had eight coupled resonators. The target straight wall nanowell had a constant void radius of 175 nm from the top to the bottom of the stack. The tapered nanowell had a void radius of 175 nm at the top tapered down to 70 nm at the bottom. As the radius was varied in both the tapered and straight walled systems, the slope of the side wall was unchanged. Both systems had a target period of 345 nm

Table 1 Comparison of the wavelength position stability in nanowell arrays made with/without side wall angle, and etched into a solid or multilayered film. The spectra of the nanowells was investigated with a top radius of 175, 177.5 (1.45 %), and 180 nm (2.9 %) with a period of 345 nm. The spectra of nanowells was also compared with periods of 345, 350 (1.45 %), and 355 nm (2.9 %) with a top radius of 175 nm. The percentages shown are the relative wavelength shifts observed under the given change in period or radius

	1.45 % change in period (%)	2.9 % change in period (%)	1.45 % change in radius (%)	2.9 % change in radius (%)
Solid gold straight nanowell	4.1	7.1	2.1	4.6
Solid gold angled nanowell	19.4	21.6	5.9	9.9
Multilayer straight nanowell	5.1	11.8	5.3	9.1
Multilayer angled nanowell	1.1	3.2	0.5	0.6

fabrication errors if the wells were spaced further apart, but the electric field intensity dropped off dramatically.

In addition to this coupled negative and positive refractive index stability, the array of sub-wavelength tapered nanowells creates a uniform surface of high field enhancements with strong broad band absorptance. All of these contributions combine to produce a fabrication error tolerant, broad band, uniform, large enhancement SERS surface with nearly flat spectral response. These improvements to the design of SERS devices could greatly enhance the spatially averaged response of a plasmonic surface, and surpass the performance limiting SERS uncertainty principle.

4 Conclusions

This study theoretically investigates the electric field enhancement from a nanowell array etched into a metal/dielectric multilayer. The structure produces significant electric field activity as the nanowells in the array approached one another. Thus, the design should produce very high Raman enhancement. Using multiple metal layers distributes the electric field in the z-direction, and broadens the enhancement bandwidth. The plasmonic absorptance of a multilayered nanowell is nearly three times stronger than a solid gold well. The side wall angle of the nanowell was varied, and larger side wall angle devices produce a strong resonator with the highest field intensities located near the top surface and a resonance wavelength position that is more resilient to fabrication imperfections. The wavelength stability of the tapered nanowell is attributed to resonators at the top and bottom of the nanowell having conflicting responses to radius/period changes. This leads to the nanowell spectral response having more stability than the solid gold structure, or the multilayer structure without side wall angle.

Acknowledgments This work was supported by the Office of Navy Research and the Office of Navy Research Independent Laboratory In-House Research funds.

References

1. S.M. Nie, S.R. Emery, Science **275**, 1102 (1997)
2. R.J.C. Brown, M.J.T. Milton, J. Raman Spectrosc. **39**, 1313 (2008)
3. J. Gersten, A. Nitzan, J. Chem. Phys. **73**, 3023 (1980)
4. L.A. Dick, A.D. McFarland, C.L. Haynes, R.P. Van Duyne, J. Phys. Chem. B **106**, 853 (2002)
5. P.L. Stiles, J.A. Dieringer, N.C. Shah, R.P. Van Duyne, Annu. Rev. Anal. Chem. **1**, 601 (2008)
6. A. Alu, N. Engheta, New J. Phys. **12**, 013015 (2010)
7. Z. Li, Z. Zhang, Phys. Rev. B **62**, 1516 (2000)
8. T.A. Klar, A.V. Kildishev, V.P. Drachev, V.M. Shalaev, IEEE J. Sel. Top. Quantum Electron. **12**, 1106 (2006)
9. G. Dolling, C. Enkrich, M. Wegener, C.M. Soukoulis, S. Linden, Opt. Lett. **31**, 1800 (2006)
10. H. Li, B.M. Cullum, Appl. Spectrosc. **59**, 410 (2005)
11. K.H. Su, Q.H. Wei, X. Zhang, Appl. Phys. Lett. **88**, 063118 (2006)
12. J. Valentine, S. Zhang, T. Zentgraf, E. Ulin-Avila, D.A. Genov, G. Bartal, X. Zhang, Nature **455**, 376 (2008)
13. S.Y. Chen, A.A. Lazarides, J. Phys. Chem. C **113**, 12167 (2009)
14. R.T. Hill, J.J. Mock, Y. Urzhumov, D.S. Sebba, S.J. Oldenburg, S.Y. Chen, A.A. Lazarides, A. Chilkoti, D.R. Smith, Nano Lett. **10**, 4150 (2010)
15. F. Falcone, T. Lopetegi, M.A.G. Laso, J.D. Baena, J. Bonache, M. Beruete, R. Marques, F. Martin, M. Sorolla, Phys. Rev. Lett. **93**, 197401 (2004)
16. Y. Luo, A. Aubry, J.B. Pendry, Phys. Rev. B **83**, 155422 (2011)
17. H. Fischer, O.J.F. Martin, Opt. Express **16**, 9144 (2008)
18. A. Kinkhabwala, Z.F. Yu, S.H. Fan, Y. Avlasevich, K. Mullen, W.E. Moerner, Nat. Photonics **3**, 654 (2009)
19. M. Moskovits, Rev. Mod. Phys. **57**, 783 (1985)
20. T.A. Kelf, Y. Sugawara, R.M. Cole, J.J. Baumberg, M.E. Abdelsalam, S. Cintra, S. Mahajan, A.E. Russell, P.N. Bartlett, Phys. Rev. B **74**, 245415 (2006)
21. G. Dolling, C. Enkrich, M. Wegener, C.M. Soukoulis, S. Linden, Science **312**, 892 (2006)
22. T. Li, H. Liu, F.M. Wang, Z.G. Dong, S.N. Zhu, X. Zhang, Opt. Express **14**, 11155 (2006)
23. V.P. Drachev, W. Cai, U. Chettiar, H.K. Yuan, A.K. Sarychev, A.V. Kildishev, G. Klimeck, V.M. Shalaev, Laser Phys. Lett. **3**, 49 (2006)
24. G.V. Eleftheriades, IEEE Microw. Wirel. Co. **17**, 412 (2007)
25. Y.B. Zheng, B.K. Juluri, X. Mao, T.R. Walker, T.J. Huang, J. Appl. Phys. **103**, 014308 (2008)

26. T. Rindzevicius, Y. Alaverdyan, B. Sepulveda, T. Pakizeh, M. Kall, J. Phys. Chem. C **111**, 1207 (2007)
27. S. Zhang, W. Fan, N.C. Panoiu, K.J. Malloy, R.M. Osgood, S.R.J. Brueck, Phys. Rev. Lett. **95**, 137404 (2005)
28. D.R. Smith, S. Schultz, P. Markos, C.M. Soukoulis, Phys. Rev. B **65**, 195104 (2002)
29. C. Lopez, L. Vazquez, F. Meseguer, R. Mayoral, M. Ocana, H. Miguez, Superlattice Microst. **22**, 399 (1997)